Vibrationally resolved cross sections and asymmetry parameters for the photoionization of N_2 with coupling between the $(3\sigma_g)^{-1}$ and the $(2\sigma_u)^{-1}$ channels

Bryan Basden and Robert R. Lucchese
Department of Chemistry, Texas A&M University, College Station, Texas 77843-3255
(Received 17 June 1987)

We have performed a vibrationally resolved two-state coupled-channel calculation using the Padé-approximant $\tilde{C}$-functional formalism for the $\nu'=0\leftarrow\nu''=0$, $\nu'=1\leftarrow\nu''=0$, and $\nu'=2\leftarrow\nu''=0$ vibrational transitions in the photoionization of N_2 leading to the $(3\sigma_g)^{-1}X^2\Sigma_g^+$ and $(2\sigma_u)^{-1}B^2\Sigma_u^+$ states of N_2^+. We have found that both the vibrationally resolved $\nu'=0\leftarrow\nu''=0$ and the vibrationally averaged asymmetry parameters in the $(2\sigma_u)^{-1}$ channel are in good agreement with vibrationally unresolved experimental data. However, the theoretical results presented here do not resolve the apparent discrepancies between the vibrationally resolved and vibrationally unresolved experimental data. Coupled-channel photoelectron asymmetry parameters and photoionization cross sections in the $(3\sigma_g)^{-1}$ channel were not found to be substantially different from earlier single-channel results. The results presented here demonstrate the need for the inclusion of further electronic correlation effects in order to give a more quantitatively accurate description of the photoionization of N_2.

I. INTRODUCTION

Electronic correlation effects between strongly coupled scattering channels are of current interest in the field of molecular-scattering theory.[1,2] This is particularly true of cases in which one or more of the scattering channels contains a shape resonance, as is the case in the molecular photoionization of N_2. The existence of a shape resonance in one channel can have a profound effect on the photoelectron asymmetry parameters and photoionization cross sections of channels to which the resonant channel is strongly coupled. The effect of the shape resonance in the photoionization channel of N_2 leading to the $(3\sigma_g)^{-1}X^2\Sigma_g^+$ state of N_2^+ on the photoionization channel leading to the $(2\sigma_u)^{-1}B^2\Sigma_u^+$ state of N_2^+ has been noted both in previous theoretical studies,[1,2] and can be seen in the experimental studies of Marr *et al.*,[3] Hamnett *et al.*,[4] Plummer *et al.*,[5] Adam *et al.*,[6] Krause *et al.*,[7] and most recently in the vibrationally resolved experimental studies of Southworth *et al.*[8]

In contrast to the coupled-channel multiple-scattering-model (MSM) calculation of Stephens and Dill[2] and previous single-channel results,[9] an accurate fixed-nuclei two-state coupled-channel calculation[1] of the photoionization of N_2 leading to the $(3\sigma_g)^{-1}X^2\Sigma_g^+$ and $(2\sigma_u)^{-1}B^2\Sigma_u^+$ states of N_2^+ gave photoelectron asymmetry parameters and photoionization cross sections in good agreement with vibrationally unresolved experiments.[3-7] However, these results did not closely match the $\nu'=0\leftarrow\nu''=0$ vibrationally resolved experimental results of Southworth *et al.*[8] In this paper we report theoretical vibrationally resolved photoelectron asymmetry parameters and photoionization cross sections for both the $(3\sigma_g)^{-1}$ and $(2\sigma_u)^{-1}$ photoionization channels of N_2. We have computed the photoionization cross section within the Born-Oppenheimer approximation. Thus we compute the photoionization dynamical coefficients at several different values of R, the internuclear separation of N_2. We then obtain the vibrationally resolved result by integrating the dynamical coefficients with the appropriate vibrational wave functions over R. The fixed-nuclei dynamical coefficients were obtained using the Padé-approximant $\tilde{C}$-functional approach.[10-14] We find that the results in the $(3\sigma_g)^{-1}$ channel are not significantly different from the single-channel results[9] in this channel. In the $(2\sigma_u)^{-1}$ channel, the vibrationally resolved asymmetry parameters remain in good agreement with vibrationally unresolved experimental results,[3-7] yet they are not substantially improved with respect to the vibrationally resolved experimental results.[8] Predictions are made for the $\nu'=1/\nu'=0$ branching ratio and $\beta_{k,\,\nu'=1\leftarrow\nu''=0}$ asymmetry parameter for photoionization leading to the $(2\sigma_u)^{-1}B^2\Sigma_u^+$ state of N_2^+.

II. CLOSE-COUPLED SCATTERING EQUATIONS

In the present work each molecular geometry is treated separately. The interaction potential between the photoelectron and the molecular ion is described with single centered expansions[9] using the frozen-core coupled-channel approximation. As in the frozen-core Hartree-Fock calculations of Lucchese, Raseev, and McKoy,[9] the target orbitals of the initial-state Hartree-Fock wave function are used unchanged in the final-state ionic target wave functions, and the initial state is the Hartree-Fock wave function.

In the multichannel scattering case considered here, the final-state wave function

$$\Psi_{cc}=\sum_{n=1}^{N_c}\Psi_{t_n}(\phi_{\vec{k}_n}) \tag{1}$$

is a linear combination (n is the channel index) of spin-adapted Slater determinants

$$\Psi_{t_n}(\phi_{\vec{k}_n})=(2)^{-1/2}(\,|\,\phi_1\alpha\phi_1\beta\cdots\phi_{t_n}\alpha\phi_{\vec{k}_n}\beta\cdots\phi_s\alpha\phi_s\beta\,|+|\,\phi_1\alpha\phi_1\beta\cdots\phi_{\vec{k}_n}\alpha\phi_{t_n}\beta\cdots\phi_s\alpha\phi_s\beta\,|\,)\ , \tag{2}$$

where the ionized electron is removed from orbital ϕ_{t_n} and N_c is the number of channels. The coupled-channel wave function is required to satisfy the projected Schrödinger equation[15]

$$\left\langle \sum_{m=1}^{N_c}\Psi_{t_m}(\delta\phi_{\vec{k}_m})\,|\,H-E\,|\,\Psi_{cc}\right\rangle=0\ , \tag{3}$$

where the electronic Hamiltonian in atomic units is

$$H=\sum_{i=1}^{N}f(i)+\sum_{\substack{i,j\\(i<j)}}^{N}\frac{1}{r_{ij}}\ , \tag{4}$$

and where N is the number of electrons, with

$$f(i)=-\tfrac{1}{2}\nabla_i^2-\sum_{\alpha}\frac{Z_\alpha}{r_{i\alpha}}\ . \tag{5}$$

In Eq. (3), the $\Psi_{t_m}(\delta\phi_{\vec{k}_m})$ are all possible variations of $\Psi_{t_m}(\phi_{\vec{k}_m})$ which can be obtained by variations in the channel scattering functions $\phi_{\vec{k}_m}$. In the multichannel case, if we make no assumption concerning the orthogonality of the continuum channel functions with the target orbitals, then Eq. (3) gives

$$\begin{aligned}0=&\langle P\,\delta\phi_{\vec{k}_m}\,|\,H^{HF}-E_m-J_{t_mt_m}+2K_{t_mt_m}\,|\,P\phi_{\vec{k}_m}\rangle\\&+\sum_{n=1}^{N_c}\langle P\,\delta\phi_{\vec{k}_m}\,|\,2K_{t_nt_m}-J_{t_nt_m}\,|\,P\phi_{\vec{k}_n}\rangle\\&+2(E^{HF}-E)\langle\delta\phi_{\vec{k}_m}\,|\,\phi_{t_m}\rangle\sum_{n=1}^{N_c}\langle\phi_{t_n}\,|\,\phi_{\vec{k}_n}\rangle\ ,\end{aligned} \tag{6}$$

where we have considered a variation of the form $\delta\phi_{\vec{k}_m}\neq0$ and $\delta\phi_{\vec{k}_n}=0$ for $n\neq m$. In Eq. (6), the operators P, H^{HF}, $J_{t_nt_m}$, and $K_{t_nt_m}$ are defined by

$$P=1-\sum_{t=1}^{s}|\,\phi_t\rangle\langle\phi_t\,|\ , \tag{7}$$

where s is the number of spatial orbitals,

$$H^{HF}=f+\sum_{i=1}^{s}(2J_{ii}-K_{ii})\ , \tag{8}$$

$$\langle\phi\,|\,J_{t_nt_m}\,|\,\phi'\rangle=\left\langle\phi(1)\phi_{t_n}(2)\left|\frac{1}{r_{12}}\right|\phi'(1)\phi_{t_m}(2)\right\rangle\ , \tag{9}$$

and

$$\langle\phi\,|\,K_{t_nt_m}\,|\,\phi'\rangle=\left\langle\phi(1)\phi_{t_n}(2)\left|\frac{1}{r_{12}}\right|\phi_{t_m}(1)\phi'(2)\right\rangle\ . \tag{10}$$

Also in Eq. (6), E_m, the energy of the continuum electron in channel m, is given by

$$E_m=E-E_m^{core}\ , \tag{11}$$

where E_m^{core} is given by

$$E_m^{core}=E^{HF}-\epsilon_m\ . \tag{12}$$

E^{HF} is the total Hartree-Fock energy (channel independent), and ϵ_m is the orbital eigenvalue of ϕ_{t_m}, defined as follows:

$$H^{HF}\phi_{t_m}=\epsilon_m\phi_{t_m}\ . \tag{13}$$

Since the result of Eq. (6) must hold for all $\delta\phi_{\vec{k}_m}$, we consider the case where $\delta\phi_{\vec{k}_m}=\phi_{t_m}$. If we then have $E^{HF}\neq E$, Eq. (6) reduces to

$$\sum_{n=1}^{N_c}\langle\phi_{t_n}\,|\,\phi_{\vec{k}_n}\rangle=0\ . \tag{14}$$

Now, if the wave function given in Eq. (1) is rewritten separating out the nonorthogonal parts, we obtain

$$\Psi_{cc}=\sum_{n=1}^{N_c}\Psi_{t_n}(P\phi_{\vec{k}_n})+(2)^{1/2}\Psi^{HF}\sum_{n=1}^{N_c}\langle\phi_{t_n}\,|\,\phi_{\vec{k}_n}\rangle\ , \tag{15}$$

where we have used the fact that the Slater determinant projects out of $\phi_{\vec{k}_n}$ any part of the function which is not orthogonal to ϕ_r with $r\neq t_n$, and that $\Psi_{t_n}(\phi_{t_n})=(2)^{1/2}\Psi^{HF}$ for all n. Now, using Eq. (14), we have that Ψ_{cc} can be written in general as

$$\Psi_{cc}=\sum_{n=1}^{N_c}\Psi_{t_n}(P\phi_{\vec{k}_n})\ . \tag{16}$$

Thus Eq. (14) is seen to imply that the nonorthogonal contribution in one channel will exactly cancel out the nonorthogonal contributions in the other channels in Ψ_{cc}. Hence, the equation for the continuum wave function given by Eq. (6) can be reduced to

$$\begin{aligned}0=&\langle P\,\delta\phi_{\vec{k}_m}\,|\,H^{HF}-E_m-J_{t_mt_m}+2K_{t_mt_m}\,|\,P\phi_{\vec{k}_m}\rangle\\&+\sum_{n=1}^{N_c}\langle P\,\delta\phi_{\vec{k}_m}\,|\,2K_{t_nt_m}-J_{t_nt_m}\,|\,P\phi_{\vec{k}_n}\rangle\ .\end{aligned} \tag{17}$$

To construct the Lippmann-Schwinger equation which is equivalent to Eq. (17), we use the channel matrix Phillips-Kleinman pseudopotential,[9,16] whose dimensions are N_c by N_c,

$$\underline{V}_Q=\underline{V}-\underline{L}\,\underline{Q}-\underline{Q}\,\underline{L}+\underline{Q}\,\underline{L}\,\underline{Q}\ , \tag{18}$$

where $\underline{L}$, $\underline{Q}$, and $\underline{V}$ are defined by

$$(\underline{L})_{nm}=\left[-\tfrac{1}{2}\nabla^2-\frac{1}{r}+E_m\right]\delta_{nm}+(\underline{V})_{nm}\ , \tag{19}$$

$$(\underline{Q})_{nm}=\left[\sum_{t=1}^{s}|\,\phi_t\rangle\langle\phi_t\,|\right]\delta_{nm}\ , \tag{20}$$

$$(\underline{V})_{nn} = -\sum_{\alpha} \frac{Z_\alpha}{r_{i\alpha}} + \frac{1}{r} + \sum_{i=1}^{s} (2J_{ii} - K_{ii}) - J_{t_n t_n} + 2K_{t_n t_n} , \tag{21}$$

and

$$(\underline{V})_{nm} = -J_{t_n t_m} + 2K_{t_n t_m} . \tag{22}$$

The matrix Lippman-Schwinger equation[11] is then

$$\phi_E = \phi_E^c + \underline{G}_c \underline{V}_Q \phi_E , \tag{23}$$

where ϕ_E and ϕ_E^c are the vectors of channel solutions and channel Coulomb waves, and $\underline{G}_c$ is the channel Coulomb Green's matrix defined by

$$(\underline{G}_c)_{nm} = \underline{G}_c(E_m)\delta_{nm} . \tag{24}$$

III. SOLUTION OF SCATTERING EQUATIONS

The multichannel $\bar{C}$ functional approach with Padé-approximant corrections,[11,12] was used in all reported calculations. Explicitly, the variational functional was

$$\underline{M}^{3}_{35}(\phi_t, \underline{r}, \phi_E^c) = \langle \phi_t \mid \underline{r} \mid \phi_E^c \rangle + \langle \phi_t \mid \underline{r}\underline{G}_c\underline{V}_Q \mid \phi_E^c \rangle + \langle \phi_t \mid \underline{r}\underline{G}_c\underline{V}_Q\underline{G}_c\underline{V}_Q \mid \phi_E^c \rangle + \sum_{\alpha,\beta} \langle \phi_t \mid \underline{r}\underline{G}_c\underline{V}_Q\underline{G}_c\underline{V}_Q \mid \alpha \rangle \langle \underline{V}_Q - \underline{V}_Q\underline{G}_c\underline{V}_Q \rangle^{-1}_{\alpha\beta} \langle \beta \mid \underline{V}_Q\underline{G}_c\underline{V}_Q \mid \phi_E^c \rangle , \tag{25}$$

where α,β are elements of a multichannel scattering basis set.

The occupied orbitals of N_2, used as the target state wave functions, were constructed from a linear combination of spherical Gaussian basis functions. The basis set was identical to that used in the calculation of Lucchese, Raseev, and McKoy.[9] The use of spherical Gaussian functions allowed us to easily express in analytic form the result of the kinetic energy and dipole velocity operators acting on the target orbitals.[17]

All of the integrals given in Eq. (25) were computed using single center expansions centered at the bond midpoint. Values for the partial-wave expansion parameters[12] were as follows.

$l_m = 30$, maximum l included in the expansion of scattering functions.

$l_s^x = 30$, maximum l included in the expansion of the scattering functions in the exchange terms.

l_i^x = maximum l included in the expansion of the occupied orbitals in the exchange terms is 16 for $1\sigma_g$, 10 for $2\sigma_g$, 10 for $3\sigma_g$, 15 for $1\sigma_u$, 10 for $2\sigma_u$, and 10 for $1\pi_g$.

$l_i^d = 60$, maximum l included in the expansion of the occupied orbitals in the direct potential.

$\lambda_m^x = 30$, maximum l included in the expansion of $1/r_{12}$ in the exchange terms.

$\lambda_m^n = 60$, maximum l included in the expansion of $1/r_{12}$ in the direct potential not including the nuclear terms.

TABLE I. Scattering basis sets used with the Padé-approximant variational expression. These basis sets correspond to the set of α and β in Eq. (25).

Symmetry	Center[a]	l	m	α's
$2\sigma_u \rightarrow k\sigma_g$	nuclei	0	0	16.0,8.0,4.0,2.0,1.0,0.7,0.4,0.1
	nuclei	1	0	1.0,0.7,0.4,0.1
	origin	0	0	2.0,1.0,0.7,0.4,0.1
	origin	2	0	2.0,1.0,0.7,0.4,0.1
$3\sigma_g \rightarrow k\sigma_u$	nuclei	0	0	16.0,8.0,4.0,2.0,1.0,0.7,0.4,0.1
	nuclei	1	0	1.0,0.7,0.4,0.1
	origin	1	0	4.0,2.0,1.0,0.7,0.4,0.1
	origin	3	0	4.0,2.0,1.0,0.7,0.4,0.1
	origin	5	0	1.0,0.7,0.4,0.1
$3\sigma_g \rightarrow k\pi_u$	nuclei	1	1	8.0,4.0,2.0,1.0,0.5,0.1
	nuclei	2	1	0.5,0.1
	origin	1	1	1.0,05
	origin	3	1	1.0,0.5
$2\sigma_u \rightarrow k\pi_g$	nuclei	1	1	8.0,4.0,2.0,1.0,0.5,0.1
	nuclei	2	1	0.5,0.1
	origin	2	1	1.0,0.5
	origin	4	1	1.0,0.5

[a]The basis functions are symmetry-adapted functions constructed from spherical Gaussian functions centered at either the nuclei or at the origin (i.e., bond midpoint).

$l_p=6$ for $3\sigma_g\rightarrow k\sigma_u$, 7 for $2\sigma_u\rightarrow k\sigma_g$, 6 for $3\sigma_g\rightarrow k\pi_u$, and 5 for $2\sigma_u\rightarrow k\pi_g$, maximum l included in the expansion of the scattering solution.

Table I gives the initial variational scattering basis sets, used in Eq. (25), which was constructed from spherical Gaussian functions of the form[12]

$$\phi^{\alpha,l,m,\vec{A}}(\vec{r})=N\,|\,\vec{r}-\vec{A}\,|^{\,l}e^{-\alpha|\vec{r}-\vec{A}|^2}Y_{lm}(\Omega_{\vec{r}-\vec{A}})\ , \qquad (26)$$

centered both at the nuclei and at the bond midpoint.

A grid for the expansion of radial functions was prepared for each molecular geometry using a grid optimization technique.[17] We used high-order Newton-Cotes integration formulas in these calculations on N_2 photoionization cross sections. These integration formulas allowed us to achieve accurate cross sections with relative errors on the order of 10^{-3} in most cases with no more than 862 grid points. The main features of the grids and integration formulae which we used are as follows: Simpson's rule was used near the nuclear center (to a distance of about 0.04 a.u. from the nuclear center) with step sizes of about 0.003 a.u.; the eighth-order Newton-Cotes integration rule was used in the region from the origin to the nuclear center with step sizes of about 0.02 a.u.; the 16th-order Newton-Cotes integration rule was used in the region from the nuclear center to the maximum extent of the grid, which was 163.8 a.u. for all nuclear geometries, with step sizes increasing asymptotically to about 0.23 a.u.

The initial variational result obtained from Eq. (25) was corrected using the $[N/N]$ Padé-approximant approach,[10] which was found to give convergence at all energies with $N\leq 3$. Channels included in the calculation were those leading to the $(3\sigma_g)^{-1}X^2\Sigma_g^+$ and $(2\sigma_u)^{-1}B^2\Sigma_u^+$ states of N_2^+. To illustrate the convergence of the Padé approximants, Table II gives as a function of N the $3\sigma_g\rightarrow k\sigma_u$ and $2\sigma_u\rightarrow k\sigma_g$ contributions of the photoelectron asymmetry parameters and cross sections in both the dipole length and velocity[9] forms for the equilibrium geometry at a photon energy of 34 eV. As has been noted previously,[13,14] this approach rapidly converges to the correct, basis-set-independent values for the partial-wave expansion used.

TABLE II. Convergence of $[N/N]$ Padé approximants for the $3\sigma_g\rightarrow k\sigma_u$ and $2\sigma_u\rightarrow k\sigma_g$ photoelectron asymmetry parameters and photoionization cross sections of N_2 at the equilibrium geometry with 34 eV photon energy.

	Cross section		Asymmetry parameter	
	Length	Velocity		
N	(Mb)	(Mb)	Length	Velocity
			$3\sigma_g\rightarrow k\sigma_u$	
0	4.0176	3.7793	1.1062	1.1241
1	4.0939	3.8117	1.1199	1.1336
2	4.1499	3.8376	1.1194	1.1333
3	4.1505	3.8381	1.1194	1.1334
			$2\sigma_u\rightarrow k\sigma_g$	
0	0.4520	0.3333	0.9573	0.9420
1	0.4351	0.3198	0.5622	0.6836
2	0.4372	0.3206	0.5269	0.6658
3	0.4374	0.3207	0.5277	0.6657

IV. VIBRATIONALLY RESOLVED CROSS SECTIONS

We have computed the fixed-nuclei dynamical coefficients[1] for the photoionization for N_2 in the dipole length form,

$$I^L_{l,m,\mu}(R)=(k)^{1/2}\langle\Psi_i(\vec{r};R)\,|\,r_\mu\,|\,\Psi^{(-)}_{f,k,l,m}(\vec{r};R)\rangle\ , \qquad (27)$$

and in the dipole velocity form,

$$I^V_{l,m,\mu}(R)=\frac{(k)^{1/2}}{\hbar\omega}\langle\Psi_i(\vec{r};R)\,|\,\nabla_\mu\,|\,\Psi^{(-)}_{f,k,l,m}(\vec{r};R)\rangle\ , \qquad (28)$$

at five internuclear separations $R=1.868$, 1.968, 2.068, 2.168, and 2.268 a.u. We integrate over nuclear coordinates using five-point polynomial interpolation to obtain fixed-nuclei dynamical coefficients at values of R other than the five given above. The cross section for going from the ground vibrational state of N_2 to the $v'=n$ vibrational state of N_2^+ is given by

$$\sigma^{L,V}_{v'=n\leftarrow v''=0}=\frac{4\pi^2}{3c}\hbar\omega\sum_{l,m,\mu}|\,\langle\chi_i^{v''=0}\,|\,I^{L,V}_{l,m,\mu}\,|\,\chi_f^{v'=n}\rangle\,|^2\ , \qquad (29)$$

where χ_i and χ_f are the initial- and final-state vibrational wave functions, respectively, $\hbar\omega$ is the photon energy, and c is the speed of light. The asymmetry parameter β_k is defined from the differential cross section for the photoelectron by

$$\frac{d\sigma^{L,V}_{v'=n\leftarrow v''=0}}{d\Omega_{\hat{k}}}=\frac{\sigma^{L,V}_{v'=n\leftarrow v''=0}}{4\pi}[1+\beta^{L,V}_{k,\,v'=n\leftarrow v''=0}P_2(\cos(\theta))]\ , \qquad (30)$$

where θ is the angle between the direction of the polarization of the light and the momentum of the electron. Equations for β_k in terms of the dynamical coefficients have been given previously.[9] Vibrational levels corresponding to $v'=0$, 1, and 2 were used to calculate the vibrationally summed cross section

$$\sigma^{L,V}_S=\sum_n\sigma^{L,V}_{v'=n\leftarrow v''=0} \qquad (31)$$

as well as the vibrationally averaged asymmetry parameter

$$\bar{\beta}^{L,V}_k=\frac{\sum_n\sigma^{L,V}_{v'=n\leftarrow v''=0}\beta^{L,V}_{k,\,v'=n\leftarrow v''=0}}{\sum_n\sigma^{L,V}_{v'=n\leftarrow v''=0}}\ . \qquad (32)$$

We have used the Rydberg-Klein-Rees (RKR) potentials of Benesch *et al.*[18] to describe the potential surface of the $X^1\Sigma_g^+$ state of N_2, and the RKR curves of Singh

and Rai[19] to describe both the $X^2\Sigma_g^+$ and $B^2\Sigma_u^+$ states of N_2^+. The potential curves were required to have zero slope at R_e, which was taken to be 1.097 68 Å for N_2, 1.116 420 Å for the $X^2\Sigma_g^+$ state of N_2^+, and 1.074 200 Å for the $B^2\Sigma_u^+$ state of N_2^+.[20] The vibrational wave functions were then obtained using the method of Cooley,[21] which gave Franck-Condon factors for transitions from the $v''=0$ $X^1\Sigma_g^+$ state of N_2 to the $X^2\Sigma_g^+$ state of N_2^+ of 0.919 for $v'=0$, 0.0764 for $v'=1$, and 0.0041 for $v'=2$ and Franck-Condon factors for transitions to the $B^2\Sigma_u^+$ state of N_2^+ of 0.881 for $v'=0$, 0.117 for $v'=1$, and 0.0020 for $v'=2$.

V. RESULTS

In Figs. 1 and 2 we give the total dipole velocity form of the cross section σ_S^V leading to the $(3\sigma_g)^{-1}X^2\Sigma_g^+$ and $(2\sigma_u)^{-1}B^2\Sigma_u^+$ states, respectively, of N_2^+ for each of the five nuclear geometries. In these figures we have only presented the velocity form of the cross section for clarity. We also note that the velocity form of the total cross section for the photoionization of N_2 has been found to be in better agreement with experimental data than the length form of the cross section.[1,9] The dramatic effects of the internuclear separation on the cross sections result from the presence of the shape resonance in the $(3\sigma_g)^{-1}$ channel, which occurs in the 25–35-eV region at the equilibrium bond length. The position of this shape resonance is seen to be very sensitive to the bond length of N_2. It is of interest to note that the coupling between the two channels causes a rise in the cross section of the $(3\sigma_g)^{-1}$ channel which is closely related to a dip in the cross section of the $(2\sigma_u)^{-1}$ channel. The dip in the $(2\sigma_u)^{-1}$ channel is shifted up in photon energy by 3–5 eV relative to the resonance in the $(3\sigma_g)^{-1}$ channel. This phenomenon might be attributed to an approximate conservation of total oscillator strength between these two channels. This effect is evident in Fig. 3, which compares the coupled and uncoupled dipole velocity form of the cross section for photoionization leading to both the $X^2\Sigma_g^+$ and $B^2\Sigma_u^+$ states of N_2^+. Here we can clearly see that the interchannel coupling enhances the cross section in the $(3\sigma_g)^{-1}X^2\Sigma_g^+$ channel at the expense of the cross section in the $(2\sigma_u)^{-1}B^2\Sigma_u^+$ channel.

In Figs. 4 and 5 we compare the total dipole length and velocity forms of the cross section, $\sigma_S^{L,V}$, with the

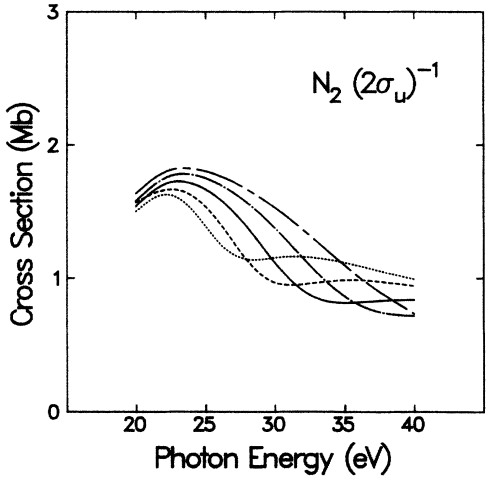

FIG. 2. Two-state coupled-channel cross sections for photoionization leading to the $(2\sigma_u)^{-1}B^2\Sigma_u^+$ state of N_2^+ at five internuclear separations in the dipole velocity approximation (same designations as in Fig. 1).

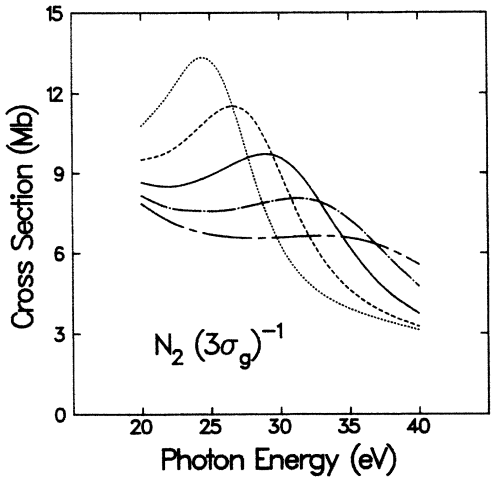

FIG. 1. Two-state coupled-channel cross sections for photoionization leading to the $(3\sigma_g)^{-1}X^2\Sigma_g^+$ state of N_2^+ at each of the five internuclear separations in the dipole velocity approximation: · · · ·, internuclear separation $R=2.268$ a.u.; — — —, $R=2.168$ a.u.; ——, $R=2.068$ a.u.; —·—·—·, $R=1.968$ a.u.; —·—·, $R=1.868$ a.u.

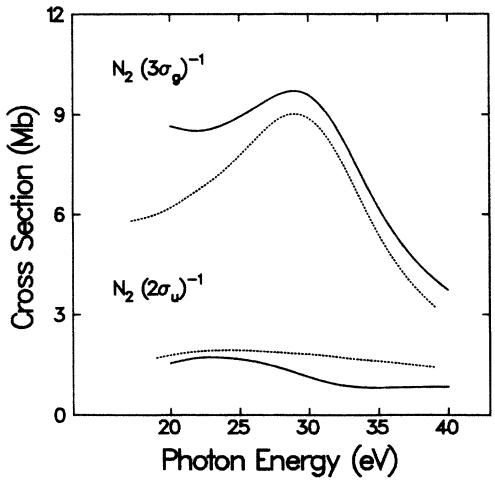

FIG. 3. Comparison of theoretical results for the photoionization cross sections of photoionization leading to both the $(3\sigma_g)^{-1}X^2\Sigma_g^+$ and $(2\sigma_u)^{-1}B^2\Sigma_u^+$ states of N_2^+: ——, two-state coupled-channel cross sections using the dipole velocity approximation; · · · ·, exact Hartree-Fock results of Lucchese *et al.* (Ref. 9).

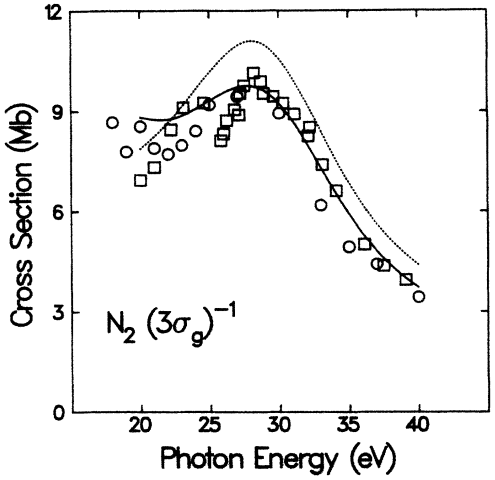

FIG. 4. Cross section for photoionization leading to the $(3\sigma_g)^{-1}X^2\Sigma_g^+$ state of N_2^+: ——, two-state coupled-channel cross sections using the vibrationally summed dipole velocity; · · · ·, two-state coupled-channel cross sections using the vibrationally summed dipole length; ○, experimental results of Hamnett *et al.* (Ref. 4); □, experimental results of Plummer *et al.* (Ref. 5).

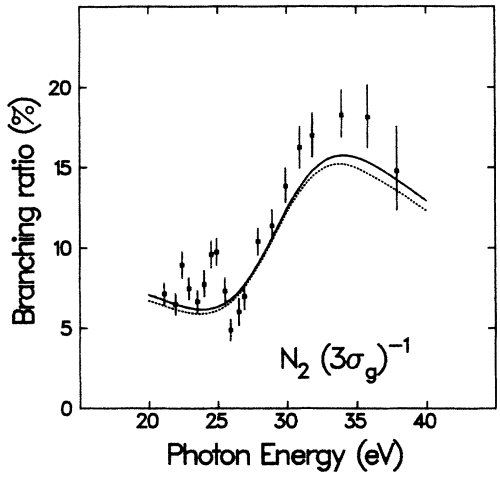

FIG. 6. Branching ratios for the $v'=1/v'=0$ vibrational levels of the $(3\sigma_g)^{-1}X^2\Sigma_g^+$ state of N_2^+ by photoionization of N_2: ——, two-state coupled-channel dipole velocity approximation; · · · ·, two-state coupled-channel dipole length approximation; ■, experimental results of West *et al.* (Ref. 22).

experimental results of Plummer *et al.*,[5] and those of Hamnett *et al.*[4] leading to both the $(3\sigma_g)^{-1}X^2\Sigma_g^+$ and $(2\sigma_u)^{-1}B^2\Sigma_u^+$ states of N_2^+. For the $(3\sigma_g)^{-1}$ channel, the coupled-channel results are in good agreement with experiment, especially in the dipole velocity form as noted above. For the $(2\sigma_u)^{-1}$ channel, the theoretical results presented here are pushed down slightly compared to earlier single-channel results,[9] but still give reasonable agreement with experiment.

Figure 6 gives the length and velocity forms of the $v'=1/v'=0$ branching ratio for the $X^2\Sigma_g^+$ state of N_2^+, as well as corresponding experimental results of West *et al.*[22] These results are in good agreement with experiment, although the effect of coupling has pushed the branching ratio down in the photon energy region of 30–35 eV when compared to earlier single-channel results.[23] In Fig. 7 we compare the $v'=1/v'=0$ branching ratio in the $(2\sigma_u)^{-1}$ channel, for photoionization leading to the $B^2\Sigma_u^+$ state of N_2^+, with the experimental data of Poliakoff *et al.*[24] In the branching ratios, we can again see the effects of the interchannel coupling to the shape resonance in the $(3\sigma_g)^{-1}$ channel. The theoretical branching ratio is in reasonable agreement with the experimental data between photon energies of 25–30 eV. However, the structure in the experimental cross section is not found in the present two-coupled-channel calcula-

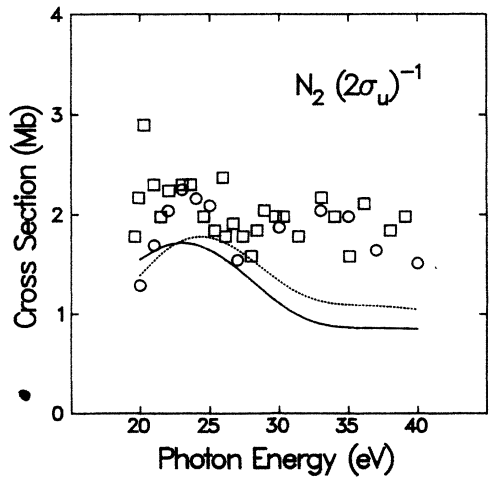

FIG. 5. Cross sections for photoionization leading to the $(2\sigma_u)^{-1}B^2\Sigma_u^+$ state of N_2^+ (same designations as in Fig. 4).

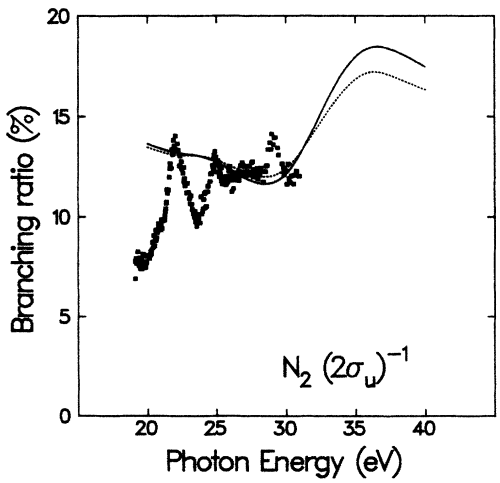

FIG. 7. Two-state coupled-channel branching ratios for the $v'=1/v'=0$ vibrational levels of the $(2\sigma_u)^{-1}B^2\Sigma_u^+$ state of N_2^+ by photoionization of N_2: ——, dipole velocity approximation; · · · ·, dipole length approximation; ■, experimental results of Poliakoff *et al.* (Ref. 24).

tion. Thus this structure is probably due to autoionization resonances which are neglected in the present calculations.

In Figs. 8 and 9 we present the vibrationally resolved asymmetry parameters, $\beta_{k,\nu'=0\leftarrow\nu''=0}^{L,V}$, and the vibrationally averaged asymmetry parameters, $\bar{\beta}_k^{L,V}$, for photoionization leading to both the $X^2\Sigma_g^+$ and the $B^2\Sigma_u^+$ states of N_2^+. These results are compared with the vibrationally resolved experimental results of Southworth *et al.*,[8] the vibrationally unresolved experimental results of Marr *et al.*,[3] and the vibrationally unresolved experimental results of Adam *et al.*[6] The channel coupling affects the asymmetry parameters in the $(3\sigma_g)^{-1}$ channel, pushing them up compared to the single-channel results.[9] As one might expect, coupling between the $(3\sigma_g)^{-1}$ and $(2\sigma_u)^{-1}$ channels has no effect on the asymmetry parameter in the 20–23-eV region, where autoionization is thought to be responsible for the feature evident in the experimental results.[5,9] The closeness of the vibrationally averaged and vibrationally resolved $\nu'=0\leftarrow\nu''=0$ asymmetry parameters in both the $(3\sigma_g)^{-1}$ and $(2\sigma_u)^{-1}$ channels is due to the dominance of the $\nu'=0\leftarrow\nu''=0$ transition as indicated by the large Franck-Condon factors of 0.919 and 0.881 for the $(3\sigma_g)^{-1}$ and $(2\sigma_u)^{-1}$ channels, respectively. As has been noted earlier,[1] the effect of channel coupling on the asymmetry parameters in the $(2\sigma_u)^{-1}$ channel is to give the desired resonant feature at photon energy of 25–35 eV. While it was hoped that vibrationally resolved $\beta_{k,\nu'=0\leftarrow\nu''=0}^{L,V}$ would be in better agreement with the $\nu'=0\leftarrow\nu''=0$ vibrationally resolved results of Southworth *et al.*[8] than the fixed-nuclei results,[1] both the vibrationally resolved and vibrationally averaged results are in good agreement with the vibrationally unresolved β's of Adam *et al.*[6] The difference between the length and velocity forms of the asymmetry parameter is fairly large compared to the discrepancy between the various experimental results.

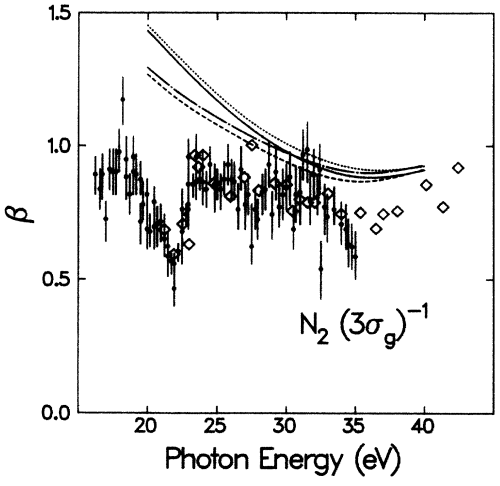

FIG. 8. Photoelectron asymmetry parameters for photoionization leading to the $(3\sigma_g)^{-1}X^2\Sigma_g^+$ state of N_2^+: ——, two-state coupled-channel vibrationally resolved $\nu'=0\leftarrow\nu''=0$ dipole velocity approximation; · · · ·, two-state coupled-channel vibrationally averaged dipole velocity approximation; — — —, two-state coupled-channel vibrationally resolved $\nu'=0\leftarrow\nu''=0$ dipole length approximation; —·—·—·, two-state coupled-channel vibrationally averaged dipole length approximation; ◇, experimental results of Marr *et al.* (Ref. 3); ●, experimental results of Southworth *et al.* (Ref. 8).

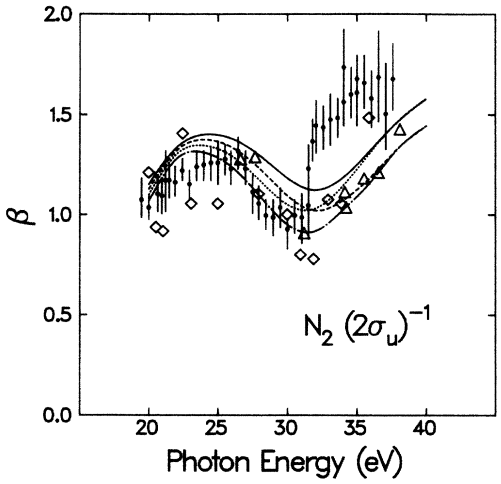

FIG. 9. Photoelectron asymmetry parameters for photoionization leading to the $(2\sigma_u)^{-1}B^2\Sigma_u^+$ state of N_2^+: ——, two-state coupled-channel vibrationally resolved $\nu'=0\leftarrow\nu''=0$ dipole velocity approximation; · · · ·, two-state coupled-channel vibrationally averaged dipole velocity approximation; — — —, two-state coupled-channel vibrationally resolved $\nu'=0\leftarrow\nu''=0$ dipole length approximation; —·—·—·, two-state coupled-channel vibrationally averaged dipole length approximation; ◇, experimental results of Marr *et al.* (Ref. 3); △, experimental results of Adam *et al.* (Ref. 6); ●, experimental results of Southworth *et al.* (Ref. 8).

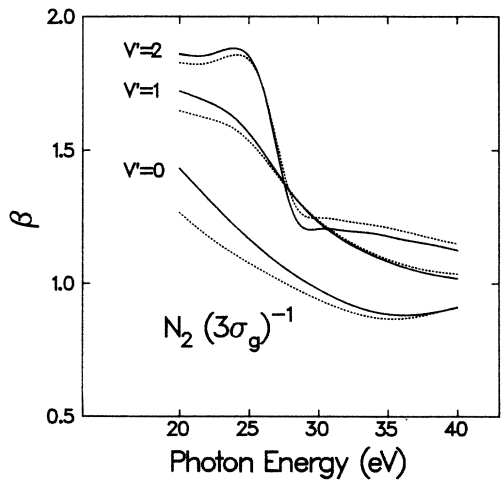

FIG. 10. Two-state coupled-channel photoelectron asymmetry parameters for photoionization of N_2 from the $\nu''=0$ state leading to the ν' vibrational level of the $(3\sigma_g)^{-1}X^2\Sigma_g^+$ state of N_2^+: ——, dipole velocity form; · · · ·, dipole length form.

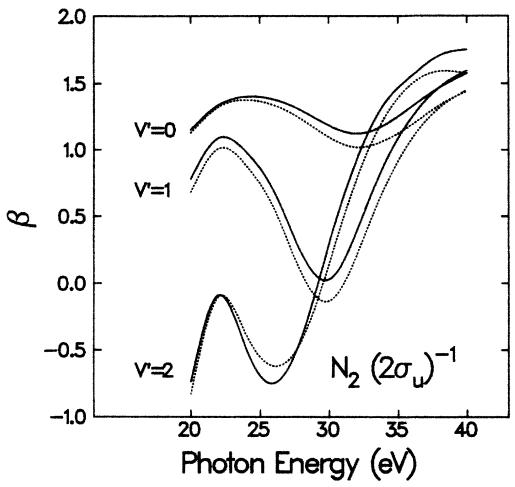

FIG. 11. Two-state coupled-channel dipole velocity photoelectron asymmetry parameters for photoionization of N_2 from the $v''=0$ state leading to the v' vibrational level of the $(2\sigma_u)^{-1}B^2\Sigma_u^+$ state of N_2^+: ——, dipole velocity form; · · · ·, dipole length form.

This indicates that further initial- and final-state correlation effects must be included in the theoretical calculation before the theory can distinguish between the experiments. We also note that there is a greater separation between the vibrationally resolved and unresolved theoretical results in the $(2\sigma_u)^{-1}$ channel than in the $(3\sigma_g)^{-1}$ channel, which demonstrates that the non-Franck-Condon effects on the asymmetry parameter are greater in the $(2\sigma_u)^{-1}$ channel. However, the separation occurs at a photon energy of 25–35 eV, rather than in the 32–40-eV region where the greatest discrepancy between the vibrationally resolved results of Southworth *et al.*[8] and the present results exists.

Figures 10 and 11 give the vibrationally resolved asymmetry parameters for the $(3\sigma_g)^{-1}$ and $(2\sigma_u)^{-1}$ photoionization channels of N_2. The $(3\sigma_g)^{-1}$ results are very similar to the single-channel results published previously.[1] The $(2\sigma_u)^{-1}$ channel asymmetry parameters show dramatic non-Franck-Condon effects. In particular, the $v'=1$ curve is substantially different from the $v'=0$ curve, especially for photon energies in the region of 25–35 eV. This difference in the vibrationally resolved asymmetry parameter explains why the largest difference between $\beta_{k,\,v'=0\leftarrow v''=0}^{L,V}$ and $\bar{\beta}_k^{L,V}$ shown in Fig. 9 also occurs for photon energies between 25 and 35 eV.

VI. CONCLUSIONS

We have found that both vibrationally resolved $v'=0\leftarrow v''=0$ and vibrationally averaged results of an accurate photoionization calculation including coupling between the $(3\sigma_g)^{-1}$ and $(2\sigma_u)^{-1}$ channels in N_2 give good agreement with vibrationally unresolved asymmetry parameters in the $(2\sigma_u)^{-1}$ channel. The results presented here indicate that vibrational resolution does not account for the discrepancy between the vibrationally resolved experimental results of Southworth *et al.*[8] and the vibrationally unresolved experimental results of Adam *et al.*[6] in this channel. For both the $(3\sigma_g)^{-1}$ and $(2\sigma_u)^{-1}$ channels of N_2, the range of experimental results and the width of error estimates associated with these results tend to suggest a need for definitive experimental studies. Photoelectron asymmetry parameters and photoionization cross sections in the $(3\sigma_g)^{-1}$ channel are largely unaffected by the coupling. The fact that the $(3\sigma_g)^{-1}$ asymmetry parameters were pushed up, and the $(3\sigma_g)^{-1}$ branching ratios were pushed down compared to experiment and to previous single-channel theoretical results[9] suggests that the two-state close-coupling approximation is necessary yet insufficient for the description of final-state electronic correlation for the photoionization of N_2. Efforts are under way to include both initial- and final-state electronic correlation in the photoionization calculations using methods such as the random-phase approximation[25] with the Padé-approximant $\tilde{C}$-functional formalism.[10–14]

ACKNOWLEDGMENTS

Acknowledgment is made to the Monsanto Company, the Dow Chemical Company Foundation, and the Celanese Chemical Company for partial support of this research. In addition, this material is based upon work supported in part by the National Science Foundation under Grant No. CHE-83-51414, and supported in part by the Robert A. Welch Foundation (Houston, TX) under Grant No. A-1020. We thank Professor M. B. Hall of Texas A&M University for use of computer codes in the generation of molecular orbitals for N_2 at the nonequilibrium molecular geometries.

[1] B. Basden and R. R. Lucchese, Phys. Rev. A **34**, 5158 (1986).
[2] J. A. Stephens and D. Dill, Phys. Rev. A **31**, 1968 (1985).
[3] G. V. Marr, J. M. Morton, R. M. Holmes, and D. G. McCoy, J. Phys. B **12**, 43 (1979).
[4] A. Hamnett, W. Stoll, and C. E. Brion, J. Electron Spectrosc. Relat. Phenom. **8**, 367 (1976).
[5] E. W. Plummer, T. Gustafsson, W. Gudat, and D. E. Eastman, Phys. Rev. A **15**, 2339 (1977).
[6] M. Y. Adam, P. Morin, P. Lablanquie, and I. Nenner, in Proceedings of the International Workshop on Atomic and Molecular Photoionization, Fritz-Haber-Institute der Max-Planck-Gesellschaft, Berlin, West Germany, 1983 (unpublished).
[7] M. O. Krause, T. A. Carlson, and P. R. Woodruff, Phys. Rev. A **24**, 1374 (1981).
[8] S. H. Southworth, A. C. Parr, J. E. Hardis, and J. L. Dehmer, Phys. Rev. A **33**, 1020 (1986).
[9] R. R. Lucchese, G. Raseev, and V. McKoy, Phys. Rev. A **25**,

2572 (1982).
[10]R. R. Lucchese and V. McKoy, Phys. Rev. A **28**, 1382 (1983).
[11]R. R. Lucchese, Phys. Rev. A **33**, 1626 (1986).
[12]R. R. Lucchese, K. Takatsuka, and V. McKoy, Phys. Rep. **131**, 149 (1986).
[13]M. T. Lee, K. Takatsuka, and V. McKoy, J. Phys. B **14**, 4115 (1981).
[14]K. Takatsuka and V. McKoy, Phys. Rev. A **23**, 2352 (1981).
[15]R. K. Nesbet, *Variational Methods in Electron-Atom Scattering Theory* (Plenum, New York, 1980), p. 9.
[16]J. D. Weeks, A. Hazi, and S. A. Rice, in *Advances in Chemical Physics* (Interscience, New York, 1969), Vol. XVI, p. 283.
[17]B. Basden and R. R. Lucchese, J. Comp. Phys. (to be published).
[18]W. Benesch, J. T. Vanderslice, S. G. Tilford, and P. G. Wilkinson, Astrophys. J. **142**, 1227 (1965).
[19]R. B. Singh and D. K. Rai, J. Mol. Spectrosc. **19**, 424 (1966).
[20]K. P. Huber and G. Herzberg, *Constants of Diatomic Molecules* (Van Nostrand Reinhold, New York, 1979).
[21]J. W. Cooley, Math. Computation **15**, 363 (1961).
[22]J. B. West, A. C. Parr, B. E. Cole, D. L. Ederer, R. Stockbauer, and J. L. Dehmer, J. Phys. B **13**, L105 (1980).
[23]R. R. Lucchese and V. McKoy, J. Phys. B **14**, L629 (1981).
[24]E. D. Poliakoff, M.-H. Ho, G. E. Leroi, and M. G. White, J. Chem. Phys. **84**, 4779 (1986).
[25]G. R. J. Williams and P. W. Langhoff, Chem. Phys. Lett. **78**, 21 (1981).